Verification of Puck's criterion for CFRP laminates under multiaxial loads at ambient and cryogenic temperatures

Jörg Hohe [a,*], Michael Schober [a], Klaus-Peter Weiss [b], Simon Appel [c]

[a] Fraunhofer Institute for Mechanics of Materials IWM, Wöhlerstr. 11, 79108, Freiburg, Germany
[b] Karlsruhe Institute of Technology, Institute for Technical Physics, Hermann-von-Helmholtz-Platz 1, 76344, Eggenstein-Leopoldshafen, Germany
[c] European Space Agency ESA/ESTEC, Structures and Mechanisms Division, Postbus 299, 2200, AG, Noordwijk, the Netherlands

ARTICLE INFO

Keywords:
CFRP laminates
Damage and failure
Cryogenic temperatures
Multiaxial loading
Puck's criterion

ABSTRACT

Objective of the present study is the verification of Puck's failure criterion for multiaxial mechanical loading situations in the ambient and cryogenic thermal regimes. The assessment is based on the material data and the failure envelope determined in a previous study on uniaxially loaded single-ply specimens study. Here, the pre-existing experimental data base is complemented by experiments on specimens made from angle ply laminates featuring holes, tapered sections and combinations thereof. The specimens were tested at ambient temperature and in a liquid Helium environment at 4.2 K. For determination of the local stress states in the individual plies at the stress concentrations induced by the holes and tapered sections, the experiments were simulated numerically by the finite element method. It is found that Puck's criterion in most cases provides conservative results. Unresolved additional safety margins may develop if a structural failure in an inter-fiber mode requires development of larger delaminations of adjacent plies to form a through crack.

1. Introduction

Fiber reinforced plastics (FRP) with carbon or glass fiber reinforcement are promising candidate materials for many types of structures to be operated in cryogenic environments. Applications include liquid oxygen and hydrogen propellant vessels for launcher systems in spacecraft technology or similar vessels for the emerging field of hydrogen technology in the automotive, rail and air transport sectors or the chemical industry (e.g. Chiao et al. [5], Choi and Sankar [6], Kumgai and Shindo [21]). Furthermore, spaceframe structures are in general exposed to cryogenic conditions, especially in missions outside the terrestrial orbit. Cryogenic environments are also found in nuclear fusion (Jin et al. [20], Miura et al. [24]), wind energy (Cormier et al. [7]) and other technologies where superconducting magnets need to be operated at extremely low temperatures.

The general advantage of fiber reinforced plastics compared to classical metallic materials is their high strength and considerable toughness even in the cryogenic regime, significantly below the ductile-to-brittle transition of all engineering metals. Especially carbon fiber reinforced plastics (CFRP) provide a high strength and stiffness. In hydrogen technology, fiber reinforced plastics provide the advantage of a low sensitivity to H_2 environments compared to most metals. Glass fiber reinforced materials (GFRP) are electrically non-conductant, making them a suitable choice in magnet technology for nuclear fusion, wind energy or other areas where superconduction and thus cryogenic environments are required (Cormier et al. [7], Jin et al. [20], Miura et al. [24]).

A major disadvantage of the application of fiber reinforced plastics in cryogenic environments is the development of substantial thermally induced stresses on the microscopic level due to the thermal mismatch between fibers and matrix. This effect occurs especially for CFRP due to the almost vanishing longitudinal coefficient of thermal expansion of carbon fibers (Abumeri et al. [1], Lord and Dutta [22]). Further residual stresses are induced in laminates consisting of unidirectional FRP plies with different orientation due to the thermomechanical anisotropy induced by the significant difference in the thermal expansions of fibers and matrix (Choi and Sankar [6]). Especially in conjunction with thermal shock and thermal gradients, the residual stresses on both fiber-matrix and laminate levels might be sufficient to trigger the formation of microcracks which eventually lead to the well-known failure of the X-33 hydrogen fuel vessel during a proof test (Niedermeyer [25]).

The effect of thermally induced microcracking of CFRP materials exposed to cryogenic temperatures has been studied by different researchers. Early studies by Adams et al. [2] and Hyer et al. [15] as well

* Corresponding author.
E-mail address: joerg.hohe@iwm.fraunhofer.de (J. Hohe).

as numerical studies by Lord and Dutta [22] date back to the 1980's. Bechel et al. [4] studied the development of leakage paths through the plies of multi-dirctional laminates caused by thermal cracking. Henaff-Gardin et al. [9] observed that under cyclic thermal loading the majority of microcracks are formed during the initial range of the load history. This finding has been confirmed in a recent study by Grogan et al. [8] who also showed that thick laminates are more sensitive to thermal loads than thin ones. These findings indicate that thermal shocking of the material might be one of the main causes for thermally induced microcracking. This hypothesis is supported by a recent study by Meng et al. [23] who observed thermally induced microcracking only under higher cooling rates whereas no such effects were observed under low cooling rates. In line with their findings, thermally induced microcracking was found only in rare cases in a recent study by the present authors (Hohe et al. [11,12]), where the specimens were cooled down carefully at low temperature rates in order to avoid the formation of any significant temperature gradients. Another reason making the integrity assessment of CFRP under crogenic thermomechanical loads different is the distinct increase of the strength of most polymeric materials in the cryogenic range (Hui and Dutta [14]) indicating that two opposing effects are active simultaneously. Therefore, the integrity assessment of CFRP materials under cryogenic conditions is a challenging task since the standard FRP failure criteria such as the Tsai-Wu [30] and Hashin [13] criteria or similar ones might be limited in their applicability. As a consequence, Shokrieh et al. [29] proposed a progressive failure model based on Hashin's criterion. A more exhaustive compilation of previous work may be found in a recent review article (Hohe et al. [10]).

The present study is concerned with the assessment of the applicability of Puck's [27,28] mechanism based FRP failure criterion to the integrity assessemnt of CFRP materials in the cryogenic temperature range. It extends a previous study (Hohe et al. [11,12]) on failure mechanisms of unidirectional CFRP materials at cryogenic temperatures to multiaxial laminates as well as to geometries with stress concentrations. In a first step, coupon specimens from angle ply laminates are characterized under tensile loads. In a second step, breadboard type specimens featuring tapered sections, holes and combinations thereof are considered in order to induce stress concentrations. In a comparative approach, all experiments are performed at ambient temperature as well as in the cryogenic regime at 4.2 K using a liquid Helium environment. The results reveal that Puck's criterion provides an accurate prediction of first ply failure under both thermal regimes although the position of failure and the active failure mechanisms might be different under both thermal regimes.

2. Material and methods

2.1. Material

As a reference material for the experimental study, a space grade CFRP material is employed. The material consists of a HexPly 8552 epoxy matrix reinforced with high strength intermediate modulus HexTow IM7 carbon fibers. Featuring a fiber volume fraction of $\rho_f = 58\%$. The material was supplied in form of plane $[\pm\alpha]_s$ angle ply laminates with 24 plies and fiber angles of 30°, 45° and 60°. All plates were manufactured by an external commercial supplier from 0.125 mm-prepreg in an autoclav process. The plate thickness was approximately 3 mm.

The material is identical to the material used in a preceeding study (Hohe et al. [11], there termed material B) and was taken from the same manufacturing batch. In the preceeding study, the material has been excessively characterized with respect to its static material response under both the ambient and the cryogenic regime. The results were employed to define the Puck [27,28] failure envelopes. A comprehensive presentation of the stiffness and strength characteristics can be found in the original contribution.

2.2. Experimental procedures

For verification of Puck's criterion [27,28], the material was tested on two levels. On the first level, coupon type specimens with smooth sides are tested under tension and compression. The characterization under tension was performed on dog-bone specimens with gauge section length and width of 30 mm and 8 mm, respectively. Dog-bone specimens could be used here since only angle-ply laminates without UD plies oriented within the loading direction were considered. The wider specimen ends provided a better clamping especially in the cryogenic environment. The compression tests were performed on rectangular specimens featuring a width of 7 mm and a length of 10 mm. Details on specimen geometry and dimensions are presented in Fig. 1. The specimens were supplied with $[\pm30°]_s$, $[\pm45°]_s$ and $[\pm60°]_s$ stacking sequences.

On the second level, tensile specimens with stress concentration features were tested. The outer dimensions of the specimens were 30 mm × 200 mm. To induce stress concentrations the breadboard specimens were supplied with holes (later referred to as type "H"), tapered sections (type "T") as well as combinations thereof (type "HT") in order to induce interactions between different stress concentration points. Both, holes and tapered sections were designed to reduce the thickness to half of the specimen width. All breadboard specimens featured a $[\pm30°]_s$ stacking sequence. Geometry and dimensions are presented in detail in Fig. 1. The specimens for both levels of the experimental characterization were manufactured from the plane laminate plates using water jet cutting.

The specimens were tested under quasi-static conditions till failure. All tensile specimens were tested in a standard tensile test rig using a mechanical wedge clamping system. The compression specimens were tested between two parallel compression platens. In order to avoid thermally induced twisting at cryogenic temperature 4.2 K away from the absolute thermal zero, no parallel motion system like a Celanese device or similar could be used. For comparison, the coupon and breadboard specimens were tested at ambient temperature and in a cryogenic environment. In order to ensure comparability, similar test devices and clamping systems were used at both test temperatures. The tests at ambient temperature were performed in a standard laboratory air environment. For the experiments in the cryogenic regime, a liquid Helium environment at $T = 4.2$ K was employed.

The experiments at ambient temperature were performed using an electromechanical Hegewald & Peschke inspect table 250 testing machine. The strain was determined by means of a tactile clip gauge. For the experiments in the cryogenic regime, a tensile hydraulic testing machine equipped with a liquid Helium bath cryostat was used [3]. To obtain the 4.2 K environment a controlled Helium filling was done to avoid thermal shock induced pre-damage to the specimens. All specimens tested under cryogenic conditions were cooled down carefully at a cooling rate of $\dot{T} \leq 1.2\,\mathrm{K/min}$. The strain measurement was performed with cryogenic calibrated clip-on extensometer [26]. The tests were performed following appropriate standard for tensile test in liquid Helium environments [18].

Although non-standard specimen geometries and thermal environments were used, the tensile and compressive experiments were performed and evaluated similar as defined in the common test standards for tensile and compressive testing of fiber reinforced materials [16,17,19] where possible. The specimens were loaded under quasi-static loading conditions till failure applying constant crosshead velocities of $v_{crosshead} = 0.5$ mm/min (cryogenic conditions) and 1 mm/min (ambient temperature). During the experiments, the crosshead displacement and the resulting force were continuously recorded. The coupon specimens were equipped with clip-on extensiometers for direct determination of the macroscopic strain in their gauge sections. In the breadboard experiments local strains were acquired in order to be able to detect local failure events. The local strain measurements were performed by a

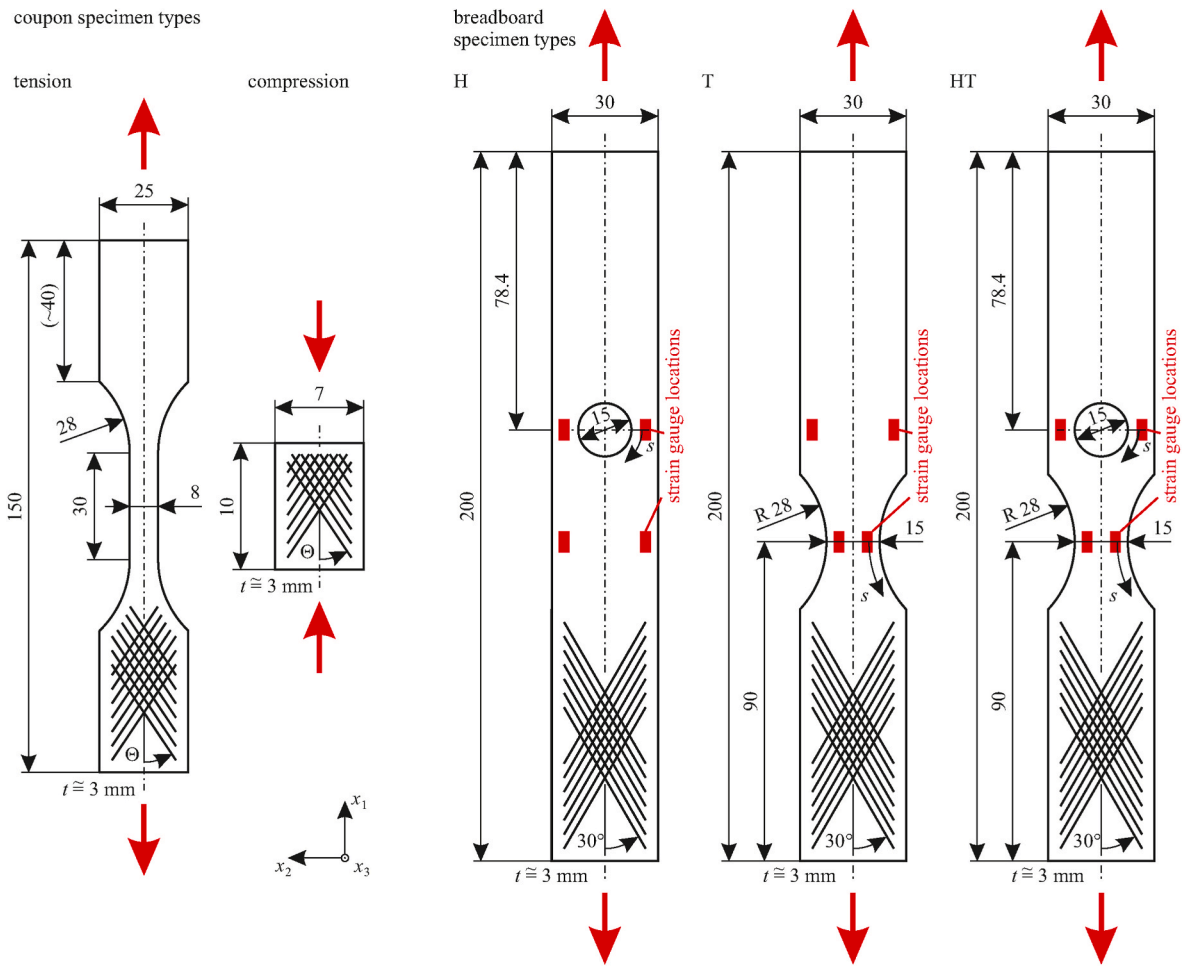

Fig. 1. Specimen types.

resistance strain gauge instrumentation on one side of the specimens tested at ambient temperature whereas special cryogenic clip-on extensiometers on both sides of the specimens were employed in the cryogenic experiments. The local strain measurements were performed on four positions located in the area of the notch roots of the holes and tapered sections or at the corresponding locations at the outer edges of the specimens which did not feature the respective stress concentration features (see Fig. 1). In the tests at ambient temperature, the local strain acquisition was complemented by a video recording for visual inspection of the opposite side of the specimen.

2.3. *Test evaluation*

The coupon experiments were evaluated in terms of their failure stresses on ply level. As usual in uniaxial tensile experiments [16], it was assumed that the stress state in their gauge sections was constant and that the longitudinal stress in both the $[+\alpha]$- and the $[-\alpha]$-plies could be determined according to $\sigma = F/A$ from the resultant force F and the cross sectional area A. Subsequently, the overall stress state σ'_{ij} with $\sigma'_{11} = \sigma$ being the only non-zero stress component was transfomed to the fiber oriented coordinate system x_i using the standard formulae of tensor transformation. The resulting local in-plane stress state (σ_{11}, σ_{22}, σ_{12}) was then evaluated against Puck's [27,28] failure envelope in the in-plane stress space which was found to be most appropriate for the considered material in a previous study (Hohe et al. [11]).

In the breadboard experiments, no constant stress state develops in the specimen plane due to the holes and tapered sections inducing stress concentrations. For this reason, a finite element simulation of the experiments has been performed. The specimens were meshed using standard 4-node plate elements with bi-linear displacement interpolation and full integration. The material was defined as a layered linear elastic orthotropic material with local orientations according to the stacking sequence. The in-plane material parameters $E_1 = 164760$ MPa, $E_2 = 8800$ MPa, $\nu_{12} = 0.295$, and $G_{12} = 5990$ MPa for the individual plies in the fiber oriented coordinate system were estimated from the experiments on unidirectionally fiber reinforced coupons of the identical material in a previous study (Hohe et al. [11]). The displacements of the nodes on the upper and lower ends of the specimens (Fig. 1) were constrained such that the specimen ends remain straight during deformation. During the deformation history, one of the specimen ends was kept fixed whereas the opposite end was loaded by a linaerly increasing force. The analysis was performed in terms of the geometrically non-linear framework, however, due to the inherent stiffness and brittleness of the material, no large strains develop prior to failure. In order to obtain proper stress results even in ranges with stress concentrations and thus steep stress gradients, a fine mesh resolution with element edge lengths between 0.2 mm down to 0.05 mm has been used. The results of the finite element analysis were evaluated in terms of the local material utilization factors $F_i (i = 1, 2, \ldots, 5)$ according to the five failure modes considered by Puck's [27,28] criterion. The material utilization factors were evaluated during the entire load history for each element and each ply in the model. Once any of the distributed material utilization factors reached a value of $F_i = 1$, first ply failure at this position and instant in time of the loading history was assumed.

3. Results

3.1. Coupon experiments

In a first test campaign, tensile and compressive coupon specimens according to Fig. 1 with different fiber orientation angles Θ were tested till failure. The results are presented in Fig. 2(a) and (b) for ambient and cryogenic temperature respectively. For information, the Puck [27,28] inter-fiber failure envelopes as obtained in a preceeding study (Hohe et al. [11]) are added together with the underlying test results on UD specimens from the aforementioned study. Further to the experiments at ambient temperature a thermocycled specimen which was cooled down to the cryogenic regime without mechanical load and reheated subsequently has been tested. For all laminates tested in the present study, the results were transformed back into a local fiber oriented coordinate system with x_1 being the fiber direction and x_2 as the second in-plane direction.

At both temperatures, the experimental results on the $[\pm\Theta]_{12}$-laminates under compression are found in a good agreement with the failure prediction by Puck's criterion, especially when considering the scatter in the UD results from the previous study on which the failure envelope is based. Under tensile loads, the Puck failure prediction is found to be highly conservative, especially for low fiber angles Θ, i.e. 30° and 45°. This effect is caused by the fact that the Puck criterion works on the single ply level and thus does not account for the delamination between adjacent plies which might be required in multidirectional laminates when the individual plies fail in a neat inter-fiber mode.

The amount of inter-ply delamination required for specimen failure at the different fiber angles Θ becomes obvious in the failure modes of the tensile specimens for the different angles presented in Fig. 3(a)–(c) (to avoid confusion, please notice that the fiber angle was counted in a different manner in the specimen labels). Especially in the failure mode of the $[\pm 30°]_{12}$ specimen in Fig. 3(c), large triangular delaminated areas are visible. Similar delaminated zones are found in all 23 ply interfaces in Fig. 3(d), whereas almost no fiber fracture is observed. Similar observations are made in the experiments on the $[\pm 45°]_{12}$ and $[\pm 60°]_{12}$ specimens. Nevertheless, much smaller delamination triangles develop in Fig. 3(a) and (b) with the delamination area approaching zero as $\Theta \rightarrow 90°$. Thus, the amount of the additional delamination work required for fracture on specimen level decreases when the fiber angle Θ approaches 90°. Consequently, decreasing conservatisms (or underestimations of the specimen failure stress) of Puck's criterion are observed in Fig. 2 (a) and (b). Similar but far less distinct observations are made in the compressive range, i.e. for $\sigma_{22} < 0$. This effect is caused by the fact that the compression specimens had a smaller width compared to their tension counterparts, keeping in mind that the area of the delamination triangles and thus the related additional fracture energy increases quadraticall with the specimen width.

Regarding the application of a preceeding thermal cycle from ambient temperature down to the liquid Helium temperature of 4.2 K and back prior to testing at ambient temperature, no effect compared to the specimens tested in the as-recieved conditions is observed in Fig. 2 (a). This result confirms the observation made in a preceeding study (Hohe et al. [11]). This result indicates that in contrast to observations reported in literature, the thermally induced residual stresses between the carbon fibers with an almost vanishing lateral thermal expansion and the matrix are not sufficiently large to cause significant microcracking for the considered material. Partially opposing observations in literature are probably due to the fact that in these studies, the specimens were mostly cooled rapidly by submersion into liquid Helium resulting in thermal shocking, whereas a careful cooling at rates of $\dot{T} \leq 1.2\,\mathrm{K/min}$ was applied in the present study.

3.2. Breadboard experiments

In a second test campaign, the breadboard specimens featuring holes ("type H"), tapered sections ("type T″) or a combination thereof ("type HT") were tested till complete failure at ambient and cryogenic temperature.

In Fig. 4(a) and (b), respectively, the load vs. cross head displacement curves for the type H breadbords at ambient and cryogenic temperature are presented. The instants in the loading history, where local failure events were identified by optical methods (ambient temperature) or from discontinuities in the local strain vs. time measurements (cryogenic temperature) are marked by symbols. At both temperatures, approximately linear load vs. displacement characteristics are obtained after an initial setting range. Due to the different clamping systems used at the different test temperatures, the extent of the setting ranges is different. At cryogenic temperature (see Fig. 4(b)), several distinct intermediate drops in the resulting force indicate slip of the specimen in the mechanical clamps rather than local failure events since the slope prior to and after the drop is identical. Although cap strips were used, slipping of the specimen in the clamps could not have been avoided due to the distinct transvers thermal contraction of the specimen when cooling down to the liquid Helium temperature of 4.2 K, resulting in the loss of clamping force. Whereas at ambient temperature, local failure events were detected mostly in the upper force range with increasing density towards the point of final fracture, two of the three specimens tested at cryogenic temperature feature local failure events in the early stage of their loading history. Nevertheless, it should be noticed that the detection of local failure events from the local strain measurements as done in the cryogenic experiments is much less robust than the visual observation of local cracking on the surface as in the tests at ambient temperature.

The failure modes of the specimens tested at ambient and cryogenic temperature are presented in Fig. 5(a) and (b), respectively. All specimens are found to fail in an inter-fiber fracture mode emanating from the notch root of the hole. At the same position, the first local failure events were observed in the visually inspected specimens tested at ambient temperature. In the same manner as in the coupon tests (Sec.

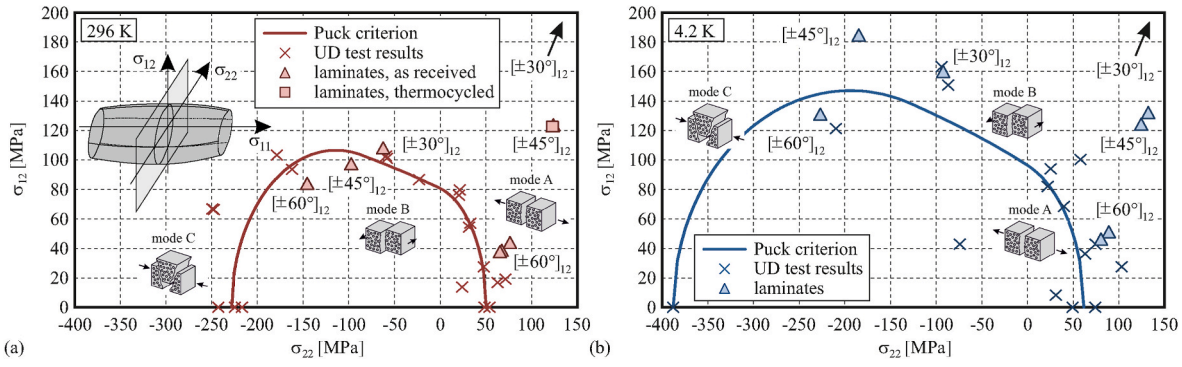

Fig. 2. Experimental results on coupon level.

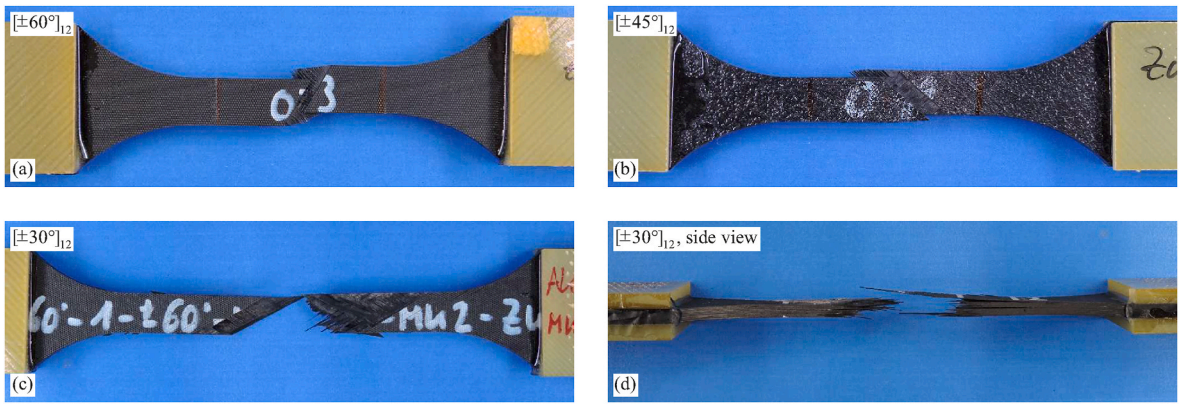

Fig. 3. Failure mode for angle-ply laminate coupons.

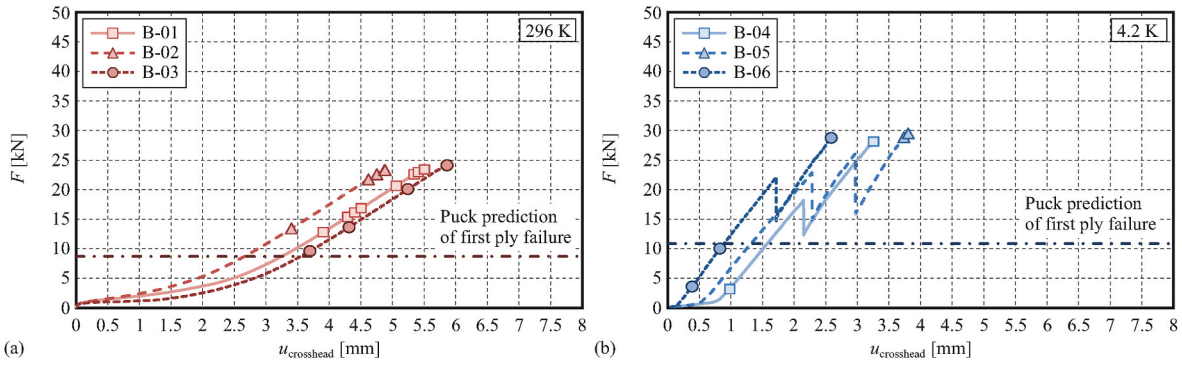

Fig. 4. Load vs. displacement characteristics – type H breadboard specimens with holes.

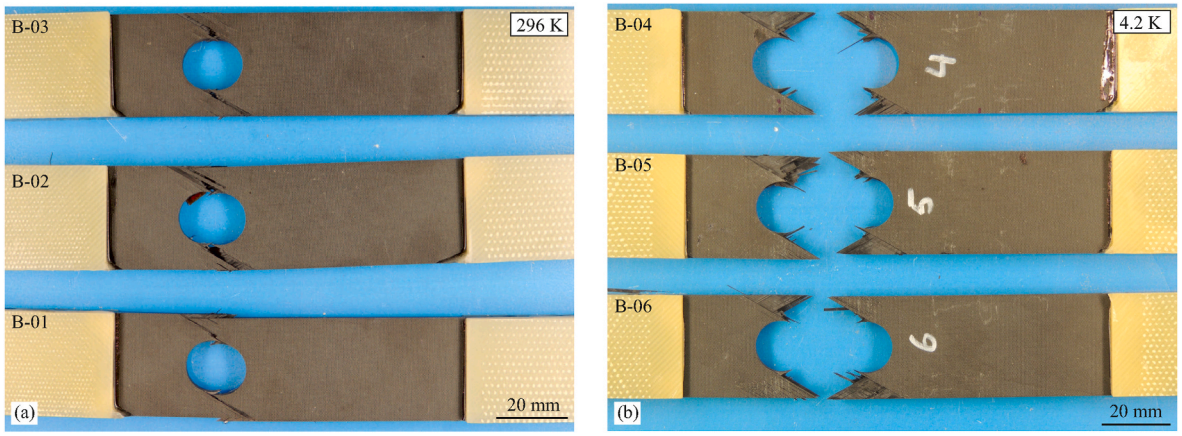

Fig. 5. Failure modes – type H breadboard specimens with holes.

3.1), the inter-fiber fracture on ply level go along with delamination of triangular regions in the interfaces of different plies with different orientation. Almost no fiber fracture is observed.

The results of a Puck failure analysis using a finite element simulation of the experiments are presented in Fig. 6. In this figure, the first line of subfigures (Fig. 6(a) and (b)) is related to the material utilization factor f_{util} whereas the second line of subfigures (Fig. 6(c) and (d))is related to the active failure mode in the respective ply. The last line of subfigures (Fig. 6(e) and (f)) is related to the stress state points along coordinate s along the inner surface of the hole. The results at ambient and cryogenic test temperatures are presented in the first and second row of subfigures, respectively. All results are presented at the instant in the loading history, where first ply failure is predicted by the criterion.

For both test temperatures, qualitatively similar results are obtained. At ambient temperature, failure is predicted to initiate at $s =$ 0.89 mm, where a hot spot of the material utilization factor f_{util} is observed. The position is in good agreement with observed failure initiation spot in Fig. 5(c). The corresponding external load level is $F = 8.73$ kN, coinciding with the observation of the first local failure events in Fig. 4(a). Failure is predicted to occurr in mode B (inter-fiber shear mode) which is predicted in Fig. 6(c) to be the active failure mode throughout most of the area of the specimen except some ranges where the compressive mode C is the active mode and a narrow range along the inner hole surface featuring a tensile active inter-fiber failure mode (mode A). Nevertheless, for both ranges, the material utilization factor f_{util} in Fig. 6 (a) is rather small, indicating that these regions are far from reaching

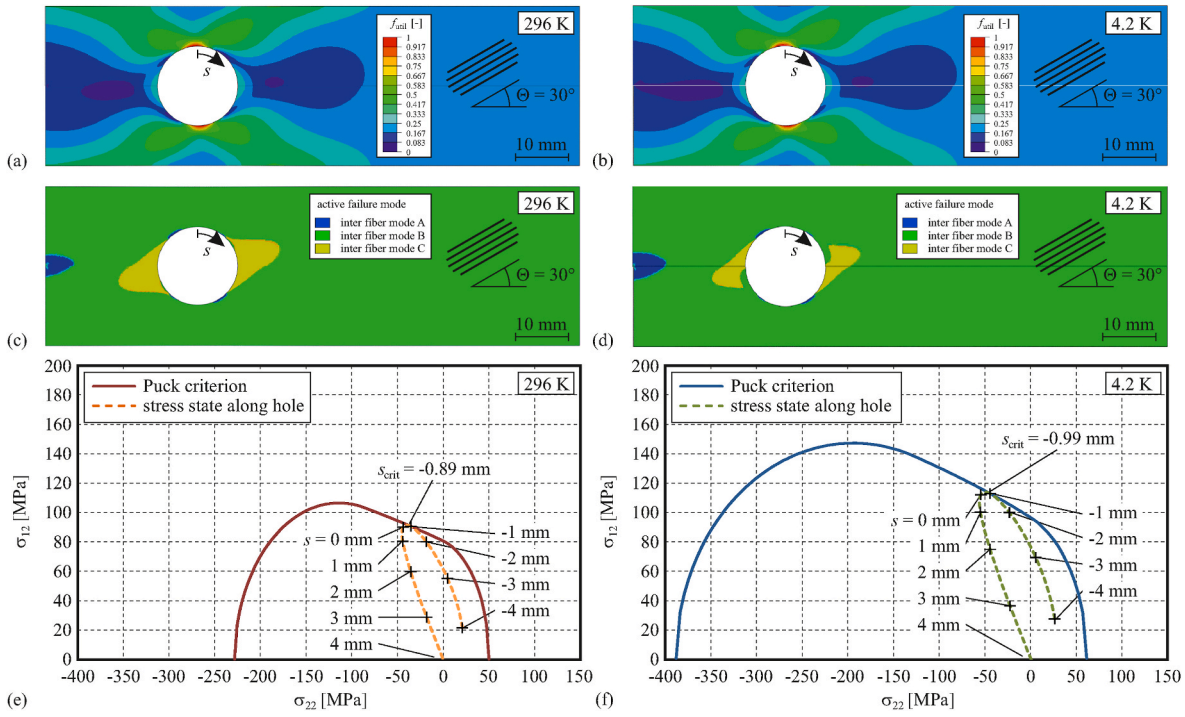

Fig. 6. Integrity assessment – type H breadboard specimens with holes.

any critical state. Qualitatively similar results are obtained at cryogenic temperature, where first ply failure is predicted in mode B at $F = 10.87$ kN occurring at $s = 0.99$ mm. Again, the prediction is found in a good agreement with the experimental observation. Thus, Puck's criterion is found to accurately predict position, load level and mode of first ply failure.

The results for the type T breadboards featuring a tapered section are presented in Figs. 7–9, arranged in a similar manner as for the results on the type H breadboards in Figs. 4–6. According to the Puck prediction, inter-fiber shear failure in mode B is the leading failure mode for first ply failure throughout most of the individual plies except for a narrow region at one end of one of the tapered sections as it can be observed in Fig. 9(c) and (d). Similar results are obtained for both test temperatures. At both, $T = 296$ K and $T = 4.2$ K, the identical position for the onset of first ply failure is predicted in Fig. 9(e) and (f), however, at different load levels due to the larger inter-fiber failure envelope at 4.2 K.

At ambient temperature, first ply failure is predicted at an axial force of $F = 17.4$ kN whereas 21.6 kN are predicted in the cryogenic range (Fig. 7). Due to the higher radius of the tapered section compared to the hole in the type H demonstrators in Fig. 4, higher failure load levels are predicted. At ambient temperature, the first local failure events on the surface were detected in the vicinity of the failure load prediction, except for specimen ES-03. Nevertheless, please notice that only local failure events on the surface rather than interior ones could have been observed. In the cryogenic range, local failure events might have occurred even below the predicted load for first ply failure. Nevertheless, it should be pointed out that the detection of local failure events from local strain measurements as performed for the tests in the liquid Helium environment is a rather difficile task. As for the experiments on the type H breadboard specimens, multiple slip of the specimen in the mechanical clamping system is observed due to the loss in clamping force induced by the transverse thermal contraction of the specimen. At both test temperatures, a significant amount of remaining stress carrying capacity beyond the first ply failure prediction is observed.

The modes of final failure are significantly different at the two test temperatures (Fig. 8). Whereas in both cases, failure is initiated in an inter-fiber shear mode as predicted by Puck's criterion, final failure of the tapered typs T specimens requires a larger amount of fiber fracture as well, since for the present [±30°] sequence, no neat inter-fiber shear crack path can be identified in the highly stressed region in the tapered section. Furthermore, moderately high loaded areas can be observed at the center line of the specimens ahead of the most narrow section in

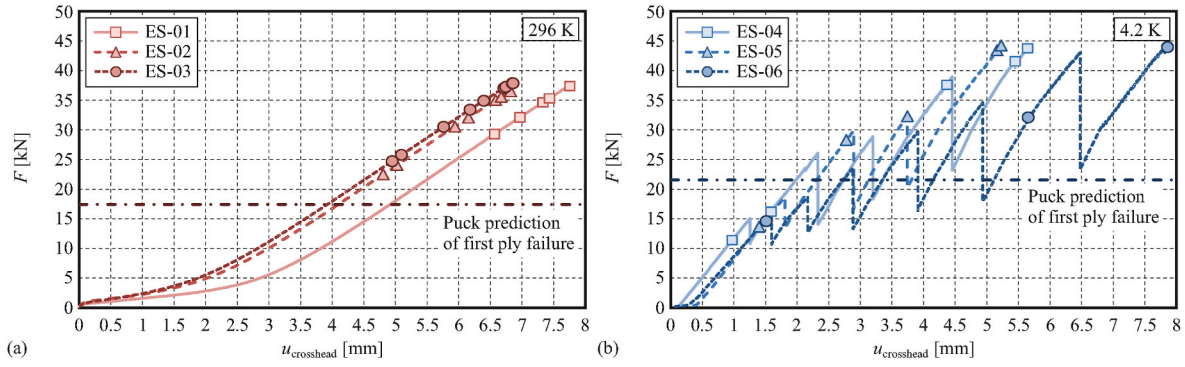

Fig. 7. Load vs. displacement characteristics – type T tapered breadboard specimens.

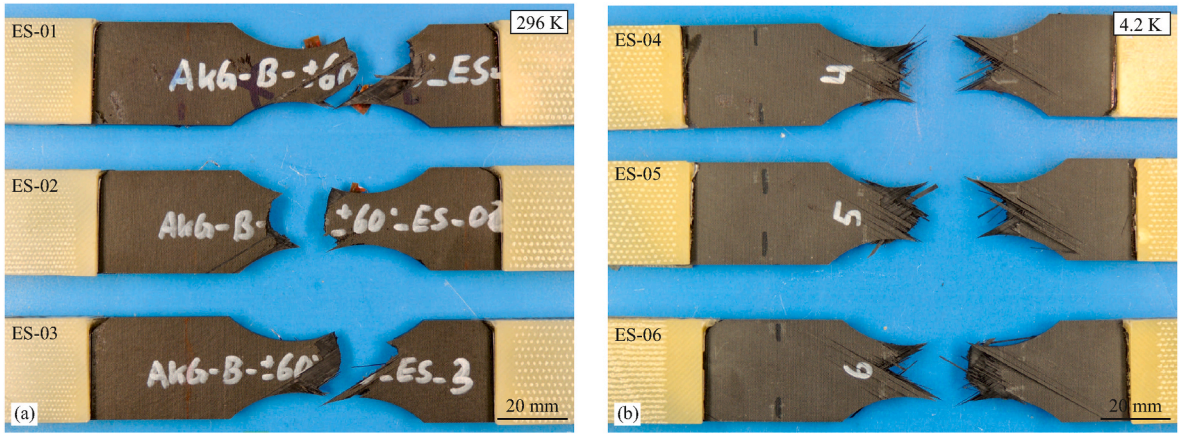

Fig. 8. Failure modes – type T tapered breadboard specimens.

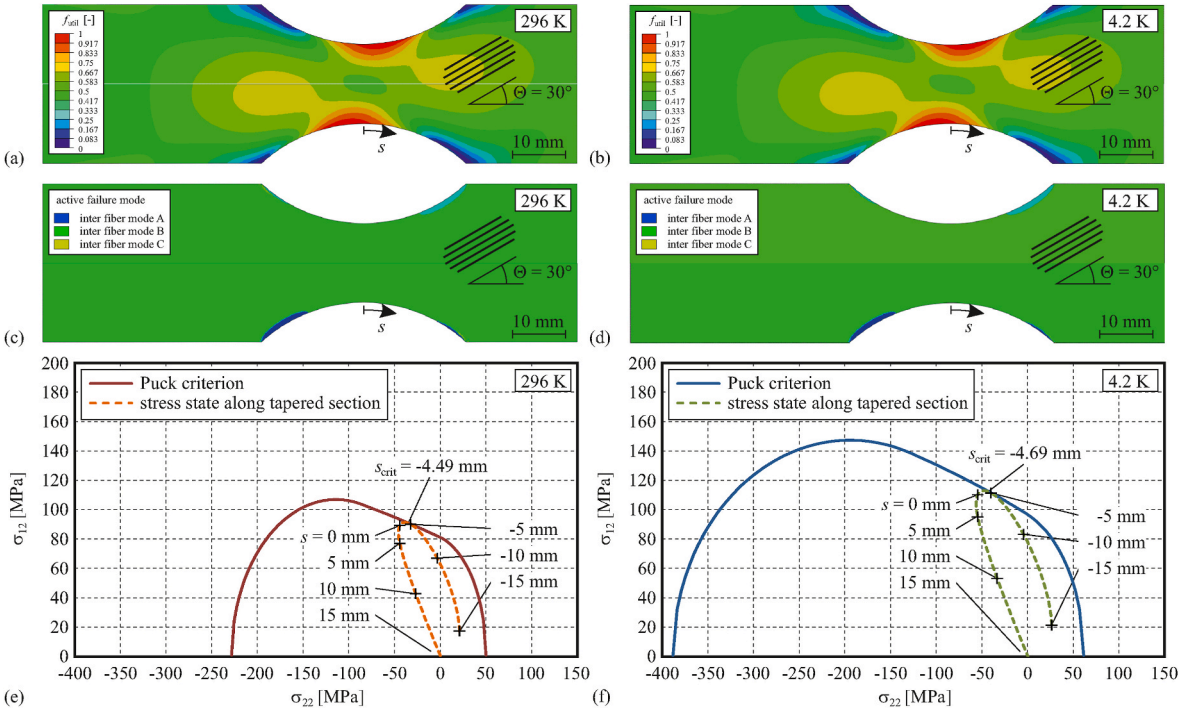

Fig. 9. Integrity assessment – type T tapered breadboard specimens.

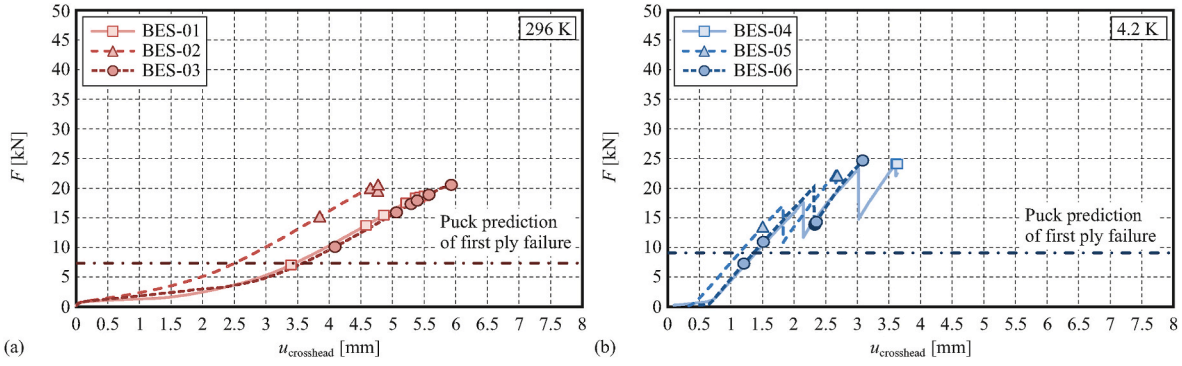

Fig. 10. Load vs. displacement characteristics – type HT tapered breadboard specimens with holes.

Fig. 9(a) and (b). Obviously, these regions are also regions of high local fiber tension. Consequently, these regions are involved in the crack path for final failure at ambient temperature in Fig. 5(a). At cryogenic temperature, no such effect is observed but final specimen failure occurs in the most narrow section of the tapered specimens (Fig. 5(b)). This change in the mode for final failure is caused by the change in the shape of the failure envelope for the different test temperatures.

The results for the type HT breadboard specimens with both features, i.e. hole and tapered section, are presented in Figs. 10–12, respectively. First ply failure is predicted in an inter-fiber shear mode (mode B) at the hole as for the type H breadboards. Nevertheless, the critical load for first ply failure is lower for the type HT breadboards than for their type H counterparts (from $F = 8.7$ kN to 7.3 kN at ambient temperature and from 10.9 kN to 9.1 kN at cryogenic temperature) due to the additional stress concentrations induced by the presence of the tapered section. Again an approximate coincidence of the first local failure events with the predicted failure load level for first ply failure is observed in Fig. 10 (a) and (b) for ambient and cryogenic test temperature, respectively. A large safety margin is observed beyond the instant of first ply failure to final failure.

As in the previous investigations, this effect is due to the requirement of the delamination of large areas of the ply interfaces for a complete separation of the specimens. Large delaminated areas for the top ply can be observed especially for specimen BES-02 tested at ambient temperature. As it is seen in Fig. 11(a) and (b), the complete separation also goes along with some fiber fracture. Nevertheless, the leading failure mode triggering specimen failure is an inter-fiber shear mode as predicted in Fig. 12. A comparison of the results of the integrity analysis of the type HT beadboard specimens with their type H and T counterparts reveals that the interaction of the two stress concentrators, i.e. hole and tapered section might also result in changes in the leading failure modes and the material utilization factors outside the critical region.

4. Discussion

In all experiments, whether on coupon level or on the level of the breadboard specimens, Puck's criterion was found to accurately predict the mode and the position of first ply failure at both ambient and cryogenic temperature. For the transition from ambient temperature and the cryogenc regime, significant changes in the size as well as in the shape of the failure envelope determined in a preceeding study (Hohe et al. [11]), i.e. the inter-fiber tensile and shear strengths increase by about 20% when the temperature is decreased from ambient temperature to the cryogenic regime whereas the inter-fiber compressive strength is nearly doubled. For this reason, the leading mode for first ply failure might change in the temperature transition. For the considered angle ply laminates, the transition of the failure mode might also involve increasing amounts of fiber fracture and thus a higher fracture energy compared to neat inter-fiber fracture. Thus, laminate designs designated for ambient temperature might not be transferred to the cryogenic regime but the cryogenic laminates might require a special design.

In all cases, a large margin of safety separates the instant of first ply failure from the final failure of the specimens. In this context, the (developing) margin of safety is defined as the force range between the force at first ply failure and the force at total failure of the respective specimen. This margin develops due to the requirement of large areas between adjacent plies for a complete separation of the specimens after inter-fiber failure of the neighboring [+ Θ] and [Θ] plies. Due to the large area to be delaminated, the separation of the adjacent plies requires a large amount of fracture energy, thus leading the safety margins observed for the type H, T and HT breadboard specimens observed in Figs. 5, 8 and 11, respectively, as well as to the distinct conservatisms in the failure prediction for the [±Θ] coupons in Fig. 2. The area to be delaminated increases with increasing size of the effective specimen width. Thus, wider specimens and structures are expected to feature more distinct effects. In the same sense, the area to be delaminated for complete separation of the specimens increases with a decreasing fiber angle Θ (see Fig. 1). It approaches zero if the fiber angle approaches 90°. Consequently, for the coupon specimens, the most distinct effect are observed for the [±30°] laminates in tension (see Fig. 2) whereas only moderate effects are obtained for the [±60°] laminates. Under compression, less distinct effects are obtained due to the smaller size of the specimens and thus the smaller delamination area. In order to utilize this effect, laminates need to be designed with a stacking sequence such that the required delamination areas become maximum. Furthermore, the use of thin ply would be advantageous due to the higher number of ply interfaces and thus a larger total delamination area compared to similar laminates with thicker individual plies but the same total thickness.

An assessment of the safety margin induced by the delamination areas would require the delamination fracture toughness, i.e. the energy release rate as additional material parameter. By this means, together with geometric considerations regarding size and shape of the required delamination zone, the work required to delaminate the respective areas could be estimated. For a complete separation, this work is necessary in addition to the failure work required for the inter-fiber fracture of the individual plies. Nevertheless, it should be noticed that this correction would depend on the respective laminate stacking sequence and the size of the specimen or structure considered. Thus, an integrity assessment based thereon is necessarily an assessment on structural rather than material level.

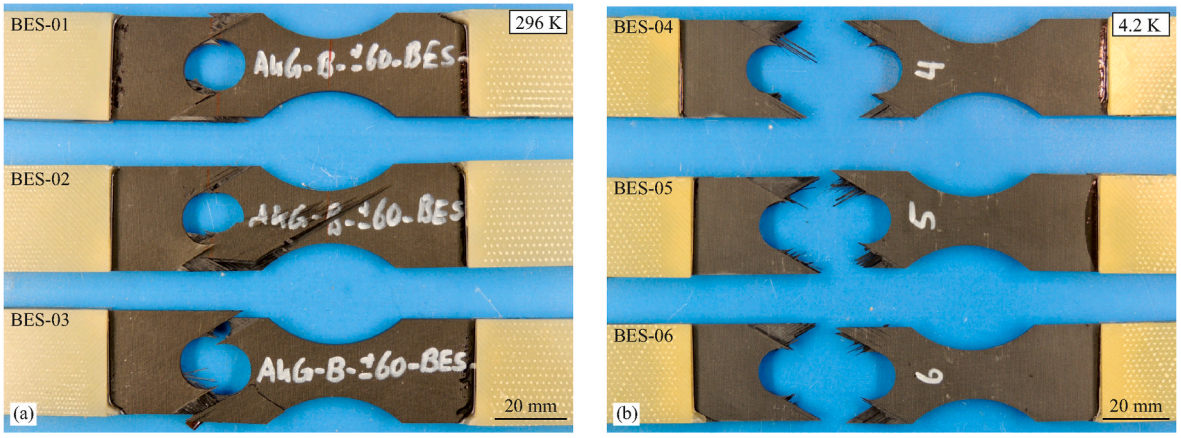

Fig. 11. Failure modes – type HT tapered breadboard specimens with holes.

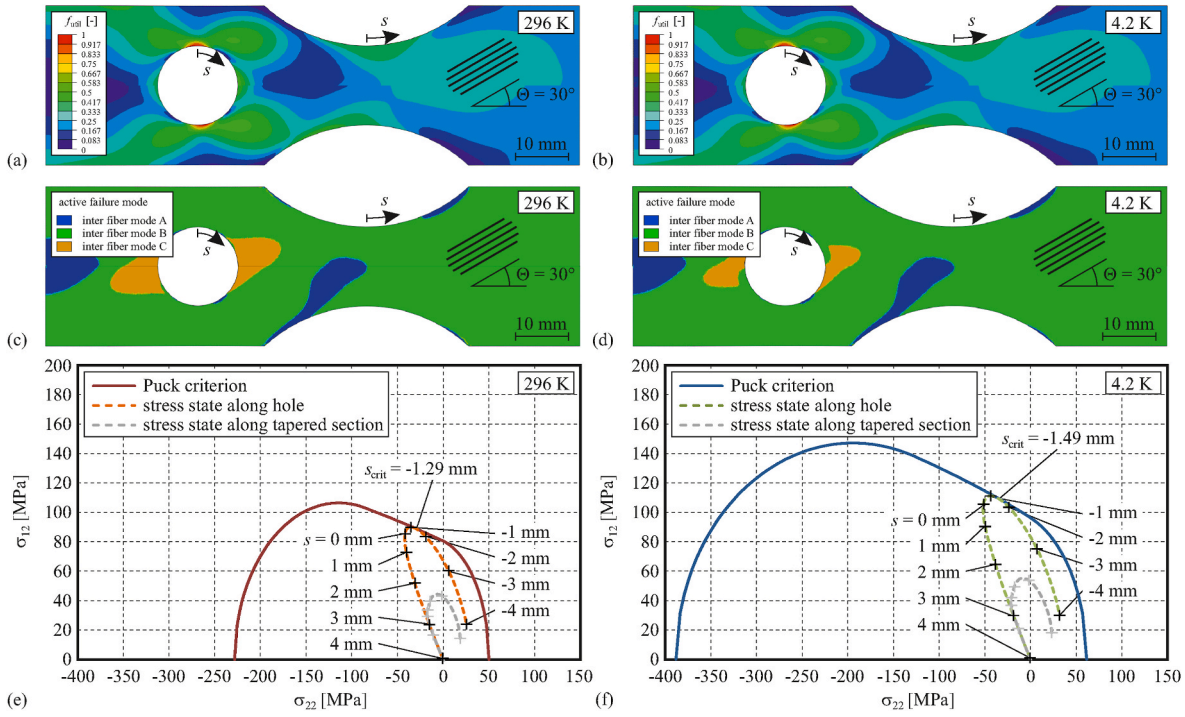

Fig. 12. Integrity assessment – type HT tapered breadboard specimens with holes.

5. Conclusions

The present study was concerned with a verification of Puck's failure criterion for CFRP laminates under ambient and cryogenic thermal environments. In an experimental approach, both coupon specimens as well as breadboard like specimens featuring tapered sections and holes were considered. By means of the tapered sections and holes, multiaxial local loading conditions were achieved. The specimens were tested at ambient temperature in a laboratory air environment as well as in the cryogenic regime using a liquid Helium environment.

At both temperatures, Puck's criterion was found to adequately predict first ply failure as the criterion works on ply level. Both, the external load and the location of the first local failure incidents were accurately predicted. For the specimens tested at ambient temperature, the local failure events were easily detected on the specimens surface by video recording of the experiments. At cryogenic temperature, no visual inspection was possible due to the liquid Helium environment. Therefore, an indirect local failure detection from local strain measurements on the specimen surface was performed. Nevertheless, the detection of local failure events proved to be difficult since local failure events in general result only in rather small pop-in's in the local strain measurements which cannot easily be distinguished from the unavoidable noise in the strain measurements.

Following the first ply failure, a significant amount of stress carrying capacity remained till the final failure event was reached. This effect is caused by the fact that first ply failure in all cases occurred in an inter-fiber fracture mode so that emerging cracks are in general bridged by the fibers of the adjacent plies. Thus, either the delamination of the ply interfaces or additional fiber fracture is required to reach final failure.

Contribution of the individual authors

J. Hohe: Conceptualization; Funding acquisition; Methodology; Project administration; Writing. M. Schober: Conceptualization; Data curation; Investigation; Validation; Visualization. K.P. Weiss: Conceptualization; Data curation; Investigation; Funding acquisition; Methodology; Validation; Visualization. S. Appel: Conceptualization; Methodology.

Declaration of competing interest

The authors declare that they have no known competing financial interests or personal relationships that could have appeared to influence the work reported in this paper.

Acknowledgements

The present work has been funded by the European Space Agency ESA under contract no. 4000118053/16/NL/BJ. The financial support is gratefully acknowledged.

References

[1] G.H. Abumeri, D.N. Kosareo, J.M. Roche, Cryogenic composite tank design for next generation launch technology, AIAA paper 2004-3390, in: Proc. 40th AIAA/ASME/SAE/ASEE Joint Propulsion Conf, 2004. Fort Lauderdale, FL, July 11-14.

[2] D.S. Adams, D.E. Bowles, C.T. Herakovich, Thermally induced transverse cracking in graphite-epoxy cross-ply laminates, J. Reinf. Plastics Compos. 5 (1986) 152–169.

[3] N. Bagrets, E. Weiss, S. Westenfelder, K.P. Weiss, Cryogenic test facility CryoMaK, IEEE Trans. Appl. Superconductivity 22 (2012), 9501204.

[4] V.T. Bechel, J.D. Camping, R.Y. Kim, Cryogenic/elevated temperature cycling induced leakage paths in PMCs, Compos. B 36 (2005) 171–182.

[5] T.T. Chiao, M.A. Hamstad, M.A. Marcon, J.E. Hanafee, Filament-wound Kevlar 49/epoxy Pressure Vessels, NASA CR-134506, Lawrence Livermore Laboratory, Livermore, CA, 1973.

[6] S. Choi, B.V. Sankar, Fracture toughness of transverse cracks in graphite/epoxy laminates at cryogenic conditions, Compos. B 38 (2007) 193–200.

[7] K. Cormier, S. Joncas, R.P.S. Nijssen, *Effects of low temperature on the mechanical properties of glass fibre-epoxy composites: static tension, compression,* $R = 0.1$ *and* $R = 1$ *fatigue of* $\pm$ [45°] *laminates*, Wind Energy 19 (2016) 1023–1041.

[8] D.M. Grogan, S.B. Leen, C.O.A. Semprimoschnig, C.M. Ó Brádaigh, Damage characterization of cryogenically cycled carbon fibre/PEEK laminates, Compos. A 66 (2014) 237–250.

[9] C. Henaff-Gardin, M.C. Lafarie-Frenot, D. Gamby, Doubly periodic matrix cracking in composite laminates Part 2: thermal biaxial loading, Compos. Struct. 36 (1996) 131–140.

[10] J. Hohe, A. Neubrand, S. Fliegener, C. Beckmann, M. Schober, K.P. Weiss, S. Appel, Performance of fiber reinforced materials under cryogenic conditions – a review, Compos. A 141 (2021), 106226.

[11] J. Hohe, M. Schober, S. Fliegener, K.P. Weiß, S. Appel, Effect of cryogenic environments on failure of carbon fiber reinforced composites, Compos. Sci. Tech. 212 (2021), 108850.
[12] J. Hohe, M. Schober, K.P. Weiss, S. Appel, Validation of Puck's failure criterion for CFRP composites in the cryogenic regime, CEAS Space J 13 (2021) 145–153.
[13] Z. Hashin, Failure criteria for unidirectional fiber composites, J. Appl. Mech. 47 (1980) 329–334.
[14] Hui, D., Dutta, P.K.: Cryogenic temperature effects on performance of polymer composites, Proc. 5th Conf. Aerospace Materials, Processes and Environmental Technology (Huntsville, AL, September 16-18, 2002).
[15] M.W. Hyer, D.E. Cooper, D. Cohen, Stresses and deformation in cross-ply composite tubes subjected to a uniform temperature change, J. Thermal Stresses 9 (1986) 97–117.
[16] ISO 527, Plastics – Determination of Tensile Properties – Part 1 to 5, 2010 (German version).
[17] ISO 604, Plastics – Determination of Compressive Properties, 1996 (German version).
[18] ISO 6892-4, Metallic Materials – Tensile Testing – Part 4: Method of Test in Liquid Helium, 2015.
[19] ISO 14126, Fibre reinforced Plastic Composites – Determination of Compressive Properties in the In-Plane Direction, 2000 (German version).
[20] H. Jin, Y. Wu, F. Long, Q.Y. Han, M. Yu, J.G. Qin, F. Liu, B.W. Tao, Mechanical properties of preliminary designed insulation for CFETR CSMC, IEEE Trans. Appl. Superconductivity 26 (2016), 9001604.
[21] S. Kumagai, Y. Shindo, Experimental and analytical evaluation of the notched tensile fracture of CFRP woven laminates at low temperatures, J. Compos. Mat. 38 (2004) 1151–1164.
[22] H.W. Lord, P.K. Dutta, On the design of polymeric composite structures for cold regions application, J. Reinf. Plastics Compos. 70 (1988) 435–458.
[23] J. Meng, Y. Wang, H. Yang, P. Wang, Q. Lei, H. Shi, H. Lei, D. Fang, Mechanical properties and internal microdefects evolution of carbon fiber reinforced polymer composites: cryogenic temperature and thermocycling effects, Compos. Sci. Tech. 191 (2020), 108083.
[24] M. Miura, Y. Shindo, T. Takeda, F. Narita, Effect of damage on the interlaminar shear properties of hybrid composite laminates at cryogenic temperatures, Compos. Struct. 93 (2010) 124–131.
[25] M. Niedermeyer, *X-33* LH_2 *tank failure investigation findings*, in: Proc. 4th Aerospace Materials, Processes and Environmental Technology Conf, 2000. Huntsville, AL, September 18-20.
[26] A. Nyilas, Strain sensing systems tailored for tensile measurement of fragile wires, Supercond. Sci. Technol. 18 (2005) 409–415.
[27] A. Puck, H. Schürmann, Failure analysis of FRP laminates by means of physically based phenomenological models, Compos. Sci. Tech. 58 (1998) 1045–1067.
[28] A. Puck, H. Schürmann, Failure analysis of FRP laminates by means of physically based phenomenological models, Compos. Sci. Tech. 62 (2002) 1633–1662.
[29] M.M. Shokrieh, M.A. Torabizadeh, A. Fereidoon, Progressive failure analysis of glass/epoxy composites at low temperatures, Strength Mat 44 (2012) 314–324.
[30] S.P. Tsai, E.M. Wu, A general theory of strength for anisotropic materials, J. Compos. Mat. 5 (1971) 58–80.